

A discrete damaging beam model for quasi-brittle fracture

M. Sage¹, J. Girardot², J.B. Kopp², S. Morel¹

¹ Université de Bordeaux, I2M umr CNRS 5295, {margaux.sage, stephane.morel}@u-bordeaux.fr

² Arts et Métiers Sciences & Technologies, I2M umr CNRS 5295, {jeremie.girardot, jean-benoit.kopp}@ensam.eu

Résumé — The aim of this work is to propose a new quasi-brittle fracture modeling based on an energy driving. In such a way, a cohesive zone model is defined here. Moreover, by reason of this ability of discontinuities simulation, the Discrete Element Method (DEM) is emphasized. An enrichment of the elastic Euler-Bernoulli beam links is realized to provide a damageable behaviour. Consequently, the necessity of a mixed mode law appears from the various bond orientations and this numerical method leads us to develop a modified cohesive zone model defined from displacements displayed by the links. To face this problem, our choice is, on the first hand, to consider tensile contribution, similarly to the conventional mode I, and on the other hand to take into account the contributions from all other loading i.e. bending, shear and torsion deformations. In order to confront our model with experimental results on quasi-brittle material, particular interest was focused on a cyclic tensile-compression test on a double notched concrete specimen. Such a test highlights the ability of the model to display the unilateral effect as well as the residual stresses during crack re-closing.

Mots clés — Méthodes aux éléments discrets, Endommagement, Critère énergétique, Rupture quasi-fragile.

1 Introduction

In recent years, the discrete element method has demonstrated its ability to model failure phenomena [1],[2], [3], [4]. Indeed, its discrete character appears to be a real advantage in the creation of discontinuities. Moreover, unlike continuous methods, this method offers the possibility of dealing with the problems of crack reclosure as well as dynamic fractures [5], [6], [7]. However, as the discrete element method is based on a lattice representation of continuous materials, continuous behaviour laws are not applicable. Indeed, the mechanical behaviour is determined via the use of a kinematic and a rheology inside a bond, like for example the elastic beam theory [1]. The failure criteria currently used remain basic. The work presented here proposes a combination of the advantages of discrete and continuous methods. To this end, a failure criterion developed for the discrete element method and inspired by the cohesive zone models used in finite elements [8], [9], [10] is elaborated. The damage beam model is implemented in the discrete element workbench *GranOO* [11].

In a first step, this damaging beam model is detailed. The reader could have more details and validation results in [12]. In the second part of the paper, the model is used to simulate a cyclic Tensile Compression test on a double notched concrete specimen. A comparison of these results with experimental tests [13] is carried out. The influence of initial internal stresses in the lattice is also studied.

2 Damaging Beam Model

First of all, the principle of discrete element method is to discretize a continuous media with particles. These discrete elements can have various shapes. The particles are connected by links which can be either springs or beams. The choice is made here to consider Voronoi elements linked by beams. An example of discretization is given in figure 1.

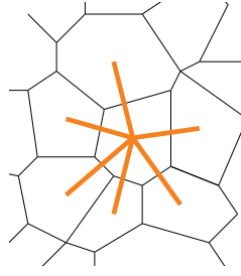


FIGURE 1 – A discretization with Voronoi discrete elements linked by beams (in orange).

Here, the mechanical behaviour of cohesive media is generated by the deformations of the lattice beams. In each of the links, the Euler-Bernouilli beam theory is applied. Thus, for each beam, three forces, one normal and two tangential forces are calculated. Likewise, three moments, one torsion and two bending moments are determined. These forces and torques are applied on each discrete element attached to the beam. The criterion inspired by the cohesive zone model proposed in this paper is an improvement of this Euler-Bernouilli beam. Indeed, in each beam, a damage variable D is defined. This variable allows to deteriorate the initial Young modulus of the beam noted E_{beam}^0 , and consequently to decrease the forces and moments, thanks to the equation (1) :

$$E_{beam} = (1 - D)E_{beam}^0. \quad (1)$$

The evolution of the damage variable D is described by an exponential law similar to the mixed mode cohesive zone model (2). Thus the damage is determined from only 3 mixed parameters (the mixity will be pointed on the all the parameters with a $\tilde{\cdot}$) : a stiffness \tilde{K} , a cohesive energy \tilde{G} and a maximum elastic displacement $\tilde{\delta}_e$. As for the classical cohesive zone models, these mixed mode parameters are deduced from the parameters of the pure fracture mode (noted I, II and III), *i.e.* stiffness, cohesive energy and maximum elastic displacement respectively for each pure mode : $K_I, G_{f,I}, \delta_{e,I}, K_{II}, G_{f,II}, \delta_{e,II}, K_{III}, G_{f,III}, \delta_{e,III}$. Finally, the current displacement in the mixed mode $\tilde{\delta}$ and its pure mode contributions δ_I, δ_{II} , and δ_{III} are defined.

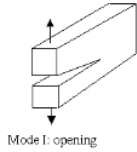
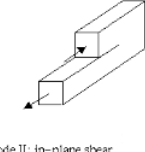
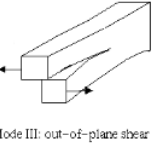
$$D = 1 - \frac{\tilde{\delta}_e}{\tilde{\delta}} \exp \left(\frac{2\tilde{K}}{2\frac{\tilde{G}}{\tilde{\delta}_e} - \tilde{K}\tilde{\delta}_e} (\tilde{\delta}_e - \tilde{\delta}) \right) \quad (2)$$

The activation of the damage evolution is governed by a mixed initiation criterion expressed as :

$$\sum_{k=I,II,III} \left(\frac{\delta_k}{\delta_{e,k}} \right)^2 = 1, \quad (3)$$

So far, the law presented above is a classical cohesive zone model already used in finite element methods. To implement it in a discrete paradigm, it remains to combine the beam theory aspect with the cohesive zone aspect. For this purpose, an analysis of the kinematics of the beams as well as an equivalence with the classical modes of failure are performed. This equivalence for each of the failure modes is illustrated in the table 1. Also, a choice is made to correspond each kinematic of the beam with a pure mode failure.

TABLE 1 – Equivalence between classical failure modes and Euler-Bernoulli beam kinematics.

Representation of classical failure modes	Corresponding beam kinematics
 <p>Mode I: opening</p>	
 <p>Mode II: in-plane shear</p>	
 <p>Mode III: out-of-plane shear</p>	

Adapting the cohesive zone model to beam theory is not trivial. In particular, mode II failure can be induced by shear loads but also by bending loads using a beam. Moreover, as the links are Euler-Bernoulli beams, a coupling between shear and bending is present making the definition of a pure mode II failure complex. Consequently, several assumptions have been made. Firstly, by studying the deformation energies of the beams during a simulation, it can be shown that most of the internal energy is due to tensile effects [1]. The torsion and bending contribution are lower. Therefore, in order to simplify the model, the choice of a mixed mode with two pseudo pure modes is adopted. The first pseudo mode of failure corresponds to the tensile effects. The second pseudo mode is assigning all other contributions : shear, bending and torsion. In this way, the pseudo mode I failure (mode I*) results from a simple difference in the length of the beam which is the first order elongation of the beam. The mode I* parameters that are proposed in this model can then be written as :

$$\left\{ \begin{array}{l} \delta_{I^*} = L - L_0 \\ K_{I^*} = \frac{E_0}{L_0} \\ \delta_{e,I^*} = \varepsilon_{e,I} L_0 \\ G_{f,I^*} = \frac{A_{beam}}{A_{vorono}} G_{f,I} \end{array} \right. \quad (4)$$

where L_0 and L are the initial and the current beam lengths and E^0 is the initial Young modulus of the beam. Note that in this definition, the energy $G_{f,I}$ is known as the fracture energy obtained from an experimental tensile test. However, due to the presence of voids within the lattice, the fracture surface associated with the fracture of a beam is not the cross section of the beam A_{beam} but the surface of the discrete Voronoi elements noted A_{vorono} . Thus, in order to take into account the lattice aspect of the domain, G_{f,I^*} is calculated from $G_{f,I}$ using the last relation in (4).

The definition of Mode II* appears to be less obvious. Mode II* displacement can be split into displacement due to torsional effects and displacement due to shear and bending effects. The torsional displacement is then expressed as a function of the torsion angle $\theta_{torsion}$ applied to the beam. Since measuring the shear and bending effects through a single displacement seems complex, the choice to introduce the

curvilinear length of the beam L_{curve} is taken. Indeed, both shear and bending effects are responsible for an elongation of the beam. Thus, a displacement defined as the difference between the curvilinear length and the length of the beam due to tensile loading can be used to monitor the shear and bending effects. Furthermore, to determine the stiffness of this pseudo mode II, a weighted average of the torsional, shear and bending stiffnesses is proposed. In addition, it should be noted that since mode II* has no physical significance, the choice of defining the maximum elastic displacement δ_{e,II^*} and the fracture energy G_{f,II^*} in proportion to the mode I* parameters is preferred. Thus, the introduction of a α parameter limits the number of parameters to be calibrated. The use of this model is then only based on input material data measured during mode I fracture tests. The calibration of a single parameter, α , through a fracture test involving mode II* fracture mechanisms like compression (see [12]), is necessary.

The equations governing mode II* are detailed in (5) :

$$\left\{ \begin{array}{l} \delta_{II^*} = L_{curve} - L + R_{beam} \theta_{torsion} \\ K_{II^*} = f_{shear} K_{shear} + f_{bending} K_{bending} + f_{torsion} K_{torsion} \\ \delta_{e,II^*} = \alpha \delta_{e,I^*} \\ G_{f,II^*} = \alpha G_{f,I^*} \end{array} \right. \quad (5)$$

$$\text{where } \left\{ \begin{array}{l} f_{shear} = \frac{F_y + F_z}{F_y + F_z + \frac{T_y}{L} + \frac{T_z}{L}} \frac{\delta_{II}}{\delta_{II^*}} \\ f_{bending} = \frac{\frac{T_y}{L} + \frac{T_z}{L}}{F_y + F_z + \frac{T_y}{L} + \frac{T_z}{L}} \frac{\delta_{II}}{\delta_{II^*}} \\ f_{torsion} = \frac{\delta_{III}}{\delta_{II^*}} \end{array} \right. \quad (6)$$

The pure modes I* and II* are defined. The parameters of the final mixed cohesive zone model can be therefore explained. The displacements, stiffness and cohesive energy of the mixed model are presented in the equation (7). The mixed mode parameters depend on the pure modes but also on the β variable quantifying the mixed rate and defined as the ratio of the mode II* to the mode I* displacements. At each iteration, the value of β is updated as well as those of the mixed law parameters.

$$\left\{ \begin{array}{l} \tilde{\delta} = \delta_{I^*} \delta_{II^*} \sqrt{\frac{1 + \beta^2}{\delta_{II^*}^2 + \beta^2 \delta_{I^*}^2}} \\ \tilde{K} = \sqrt{\frac{K_{I^*}^2 + \beta^2 K_{II^*}^2}{1 + \beta^2}} \\ \tilde{\delta}_e = \delta_{e,I^*} \delta_{e,II^*} \sqrt{\frac{1 + \beta^2}{\delta_{e,II^*}^2 + \beta^2 \delta_{e,I^*}^2}} \\ \tilde{G}_f = \frac{\delta_{II^*}^{e^2}}{\delta_{II^*}^{e^2} + \beta^2 \delta_{I^*}^{e^2}} G_{f,I^*} + \frac{\beta^2 \delta_{I^*}^{e^2}}{\delta_{II^*}^{e^2} + \beta^2 \delta_{I^*}^{e^2}} G_{f,II^*} \end{array} \right. \quad (7)$$

with

$$\beta = \frac{\delta_{II^*}}{\delta_{I^*}} \quad (8)$$

3 Closure Model

In order to be able to simulate complex loadings such as cyclic tensile compressive tests, the damaging beam model must be combined with a reclosure model. Indeed, when a quasi-brittle material damaged

in tension is subjected to a loading in compression, the micro-cracks within the material will close. In our model, the presence of these micro-cracks is introduced by the damage of the beams degrading the Young modulus. These crack reclosure mechanisms are illustrated on a macroscopic scale by a behaviour in compression similar to the behaviour of a non-damaged material. Thus, in the stress-strain response of the material, in compression, the slope corresponds to the initial Young modulus E_0 and not to the degraded Young modulus resulting from the tensile stage. To model this phenomenon, the addition of closure force and moment is proposed here. The closure forces and moments are determined so that the sum of the contributions due to the reclosure and the damaged beam is identical to that of the initial intact beam. The relation (9) is then ensured :

$$\begin{Bmatrix} \vec{F} \\ \vec{M} \end{Bmatrix} = \begin{Bmatrix} \vec{F}_{Damagebeam} \\ \vec{M}_{Damagebeam} \end{Bmatrix} + \begin{Bmatrix} \vec{F}_{closure} \\ \vec{M}_{closure} \end{Bmatrix} \quad (9)$$

In addition, micro-crack reclosure occurs within the entire representative elementary volume (REV) modelled by the reclosed beam. It is therefore necessary to take into account the part of the REV represented by voids. Thus, during the reclosure of two discrete elements, the forces $F_{closure}$ are transmitted along a surface that does not correspond to the surface of the beam but to the Voronoi surface common to both elements. The stiffness of the reclosure force $F_{closure}$ can be expressed as (10).

$$K_{closure} = D \frac{E_0 A_{vorono}}{L_0} \quad (10)$$

The prediction of the unilateral effect occurring during cyclic tests is expected by adding these forces and moments of reclosure. However, irreversible mechanisms such as inelastic deformations occurring during successive tension-compression cycles cannot be reproduced by this reclosure model. In order to observe these inelastic deformations, the choice is made to add internal constraints initially in the lattice. Thus, when the beams fail, the internal stresses are released and additional energy is dissipated. The internal stresses are obtained during the creation of the specimen. Indeed, during the elaboration of a specimen, the discrete elements are added one by one until a coordination number of 6.2 is obtained, corresponding to a random close packing. The requirement of such a coordination number implies an initial interpenetration of the discrete elements with their neighbors. Classically, a relaxation phase of the specimen allows to make these interpenetrations disappear. In order to obtain internal stresses, the relaxation phase is interrupted during the process when a certain average interpenetration in the specimen, here approximately 0.015%, is reached.

4 Results

In order to test our model, it is confronted with multiple qualitative and experimental results in [12]. Here, the focus is on a cyclic tension-compression test on a double notched concrete specimen. The geometry and dimensions of the specimen used in the test in [13] are shown in the figure 2. It should be noted that an experimental cyclic test on such a specimen required a servo-controlled loading in order to have full control over the driving in the post-peak phase. Similarly, to numerically avoid the same failure instabilities during the post-peak phase, the choice was made to reduce the height of the specimen, thus reducing the energy in the system. As the failure mechanisms take place in the area close to the notches, this assumption has no influence on the failure behaviour of the specimen. The numerical specimen and its dimensions are presented in the figure 3.

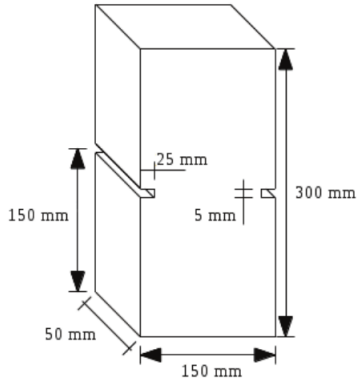


FIGURE 2 – Scheme of the specimen used in the cyclic test [13].

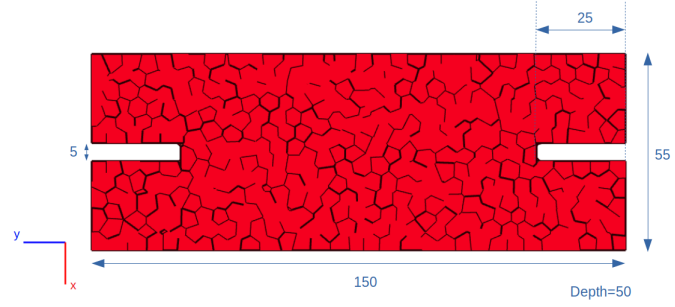


FIGURE 3 – Numerical specimen used in the cyclic test simulation (dimensions are in mm).

In addition, the specimen is composed of 5,000 Voronoi discrete elements, ensuring adequate elastic behaviour. The elastic properties obtained after calibration (*i.e.* Young modulus E_μ , poisson ratio ν_μ and the radius ratio r_μ of the beam) and the parameters of the damage model used to simulate the test are listed in the tables 2 and 3 respectively.

TABLE 2 – Material properties \cdot_M and lattice properties \cdot_μ obtained from the elastic calibration.

Material Properties	Lattice Properties
$E_M = 37.9 \text{ GPa}$	$E_\mu = 182.29 \text{ GPa}$
$\nu_M = 0.2$	$\nu_\mu = 0.3$
	$r_\mu = 0.6$

TABLE 3 – Input parameters of the damaging beam model.

Damage Parameters	
$G_{f,I}$	101 J.m^{-2}
$\varepsilon_{e,I}$	$7.18 \cdot 10^{-5}$
α	8

The stress-strain response obtained with the damaging beam model for a cyclic tensile test on a specimen with no internal stresses is presented in the figure 4. A sensitivity study was performed on the internal stresses in order to calibrate the inelastic deformation obtained numerically to the experimental value extracted from [13]. The average internal stress selected has approximately a value of 64 kPa. The stress-strain response obtained for a cyclic Tensile-Compression test with the damaging beam model and internal stresses is compared to the result without internal stresses in the figure 4.

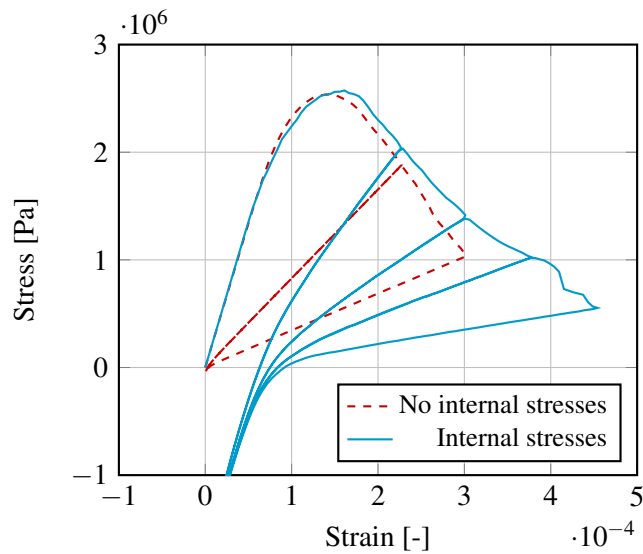


FIGURE 4 – Stress-Strain response obtained from DBM for a cyclic tensile test on a double notched specimen.

First, the onset of the damage phase appears for the same strain $\epsilon_{e,I}$ experimentally and with the model. The softening envelope obtained with the model is similar to the experimental results. In addition, the unilateral effect is observed. In the compression stage after tensile damage, the slope exhibited corresponds to the initial stiffness of the specimen.

Therefore, the influence of the initial internal stresses is noticeable in the inelastic deformations displayed during the compression stage. Indeed, the model without internal stresses is not able to reproduce inelastic deformations. The presence of stresses also has an impact on the stiffness of the damaged material. Indeed, the slopes displayed during successive discharges are predicted more accurately with internal stresses. During the first two unloadings in the simulation, the inelastic deformations agree with those observed experimentally. However, when a larger number of cycles is reached, the inelastic deformations displayed are insufficient. This observation is confirmed by the evolution of the inelastic deformation with the damage illustrated in the figure 5.

Indeed, when the damage variable is less than 0.6, the simulation with internal stresses exhibits the same inelastic deformation as experimentally. For the first four cycles, the simulation with internal stresses is faithful to the experimental results. Similarly, for the first few cycles, the evolution of the damage as a function of the proportion of fracture energy $G_{f,i}$ used in the cycle number i compared to the total fracture energy $G_{f,tot}$ is identical for the simulation with internal stresses and the experimental results as shown in the figure 5. However, when the specimen is more severely damaged, experimentally a significant increase of the inelastic deformation is observed contrary to the numerical simulation. Note also that when the specimen is highly damaged, the energy dissipated experimentally is larger than numerically. The internal stresses therefore seem to influence only the first few cycles of the test. Once these stresses are released, numerically, there is no additional energy dissipated. These results highlight the combination of these internal stresses with another predominant dissipative mechanism when the material is highly damaged. This dissipative mechanism can be attributed to frictional effects taking place between the crack lips. Indeed, in such a case, the cracking zones are larger and the friction effects are exacerbated. Thus, our DBM model could be improved in future works by taking into account frictional effects.

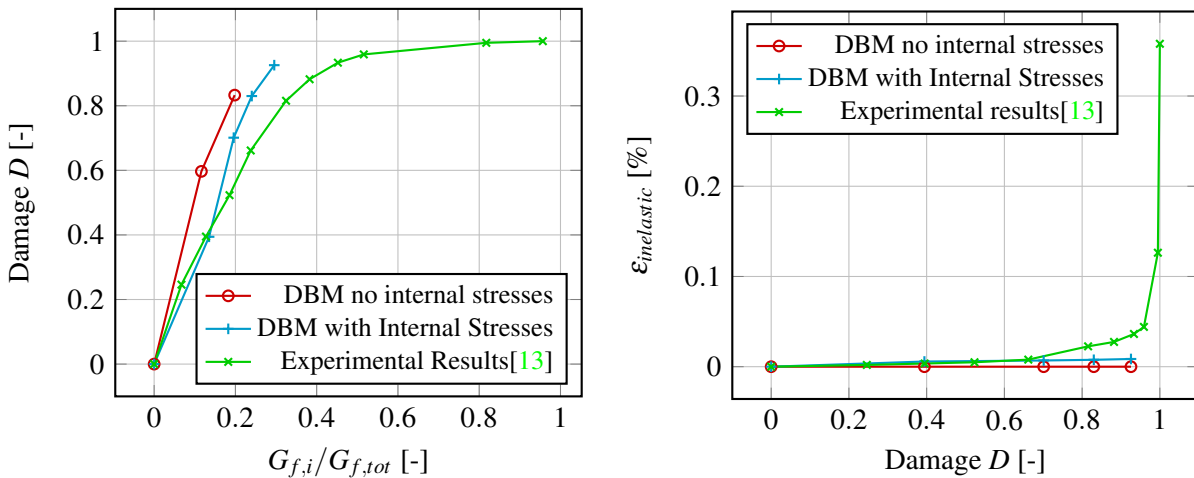


FIGURE 5 – Evolution of the damage as a function of the ratio of energy dissipated in cycle i and of the total energy dissipated (left) and the inelastic deformation regarding the damage evolution (right).

5 Conclusion

A damage model inspired by cohesive zone models applied to the discrete element method has been presented here. This study highlights the fact that damaging behaviour within a lattice leads to damaging behaviour macroscopically. Furthermore, the ability of the model to display this behaviour even for specimens composed of few elements (i.e. 5000) has been shown. In addition, the mechanisms acting during crack reclosure such as the unilateral effect are reproduced by the model. Finally, the inelastic deforma-

tions resulting from the cycling of the loading can be modelled by adding internal stresses initially in the lattice. However, this last point could be improved by taking into account the frictional effects occurring within the material.

Références

- [1] Damien André, Mohamed Jebahi, Ivan Iordanoff, Jean luc Charles, and Jérôme Néauport. Using the discrete element method to simulate brittle fracture in the indentation of a silica glass with a blunt indenter. *Computer Methods in Applied Mechanics and Engineering*, 265 :136–147, 2013.
- [2] Benjamin Schneider, Manfred Bischoff, and Ekkehard Ramm. Modeling of material failure by the discrete element method. *PAMM*, 10(1) :685–688, 2010.
- [3] E. Schlangen and E.J. Garboczi. Fracture simulations of concrete using lattice models : Computational aspects. *Engineering Fracture Mechanics*, 57(2) :319–332, 1997.
- [4] Xiaofeng Gao, Georg Koval, and Cyrille Chazallon. A Discrete Element Model for Damage and Fatigue Crack Growth of Quasi-Brittle Materials. *Advances in Materials Science and Engineering*, 2019 :1–15, February 2019.
- [5] A. Coré, J.-B. Kopp, J. Girardot, and P. Viot. Study of the dynamic fracture of hollow spheres under compression using the discrete element method. *Procedia Structural Integrity*, 13 :1378–1383, 2018. ECF22 - Loading and Environmental effects on Structural Integrity.
- [6] Mariotti, C., Michaut, V., and Molinari, J. F. Modeling of the fragmentation by discrete element method. *DYMAT - International Conference on the Mechanical and Physical Behaviour of Materials under Dynamic Loading*, 2 :1523–1528, 2009.
- [7] Yi-Lin Gui, Ha H. Bui, Jayantha Kodikara, Qian-Bing Zhang, Jian Zhao, and Timon Rabczuk. Modelling the dynamic failure of brittle rocks using a hybrid continuum-discrete element method with a mixed-mode cohesive fracture model. *International Journal of Impact Engineering*, 87 :146–155, 2016. SI : Experimental Testing and Computational Modeling of Dynamic Fracture.
- [8] Vincent Venzal, Stéphane Morel, Thomas Parent, and Frédéric Dubois. Frictional cohesive zone model for quasi-brittle fracture : mixed-mode and coupling between cohesive and frictional behaviors. *International Journal of Solids and Structures*, 2020.
- [9] M. J. van den Bosch, P. J. G. Schreurs, and M. G. D. Geers. A new cohesive zone model for mixed-mode decohesion. In E. E. Gdoutos, editor, *Fracture of Nano and Engineering Materials and Structures*, pages 973–974, Dordrecht, 2006. Springer Netherlands.
- [10] T. Vandellos, E. Martin, and Dominique Leguillon. Comparison between cohesive zone models and a coupled criterion for prediction of edge debonding. In *16th European Conference on Composite Materials*, SEVILLE, Spain, June 2014.
- [11] Damien André, Jean luc Charles, Ivan Iordanoff, and Jérôme Néauport. The granoo workbench, a new tool for developing discrete element simulations, and its application to tribological problems. *Advances in Engineering Software*, 74 :40–48, 2014.
- [12] Margaux Sage, Jérémie Girardot, Jean-Benoît Kopp, and Stéphane Morel. A damaging beam-lattice model for quasi-brittle fracture. *International Journal of Solids and Structures*, page 111404, January 2022.
- [13] Olivier Nouailletas, Christian La Borderie, Céline Perlot-Bascoules, Patrice Rivard, and Gérard Balivy. Experimental Study of Crack Closure on Heterogeneous Quasi-Brittle Material. *Journal of Engineering Mechanics - ASCE*, 141(11) :04015041, 2015.